

Article

Photochemical Release of Dissolved Organic Nitrogen from Algal Detritus and Sediment Particles in Lake Taihu, China

Yanan Liu ^{1,2} and Xiaolong Yao ^{1,*}

¹ State Key Laboratory of Lake Science and Environment, Nanjing Institute of Geography and Limnology, Chinese Academy of Sciences, Nanjing 210008, China; liuyn@stu.hbnu.edu.cn

² College of Urban and Environmental Sciences, Hubei Normal University, Huangshi 435002, China

* Correspondence: xlyao@niglas.ac.cn

Abstract: Solar irradiation in aquatic systems can induce the conversion of substances from the solid to the dissolved phase (photodissolution). Yet, the photochemical release of dissolved organic nitrogen (DON) from internal particles in lakes remains largely unknown. In this study, suspensions of algal detritus and sediment particles from a shallow eutrophic lake were exposed to simulated solar irradiation, and the release and compositional changes of dissolved organic matter were explored by measuring their UV–Visible absorption spectroscopy and ultrahigh resolution Fourier transform ion cyclotron resonance mass spectrometry (FT-ICR MS). The photochemical release of inorganic nitrogen during the incubations was also investigated. Results showed that light irradiation induced stronger dissolved organic carbon and DON production in the algal detritus suspensions, with release rates of $1.17 \text{ mg C L}^{-1} \text{ h}^{-1}$ and $0.14 \text{ mg N L}^{-1} \text{ h}^{-1}$, respectively, at an algal detritus concentration of 0.1 dry g L^{-1} . Light irradiation also induced compositional changes of DON in both algal and sediment suspensions. A larger number of DON molecules with lower molecular weight were continuously released in the algal suspensions, e.g., the total number of DON formulas increased from 1349 to 4135 during an 8 h irradiation. In contrast, upon irradiation of sediment suspensions, DON showed decreased molecular diversity and increased aromaticity. The photochemical release of ammonium (photoammonification) was also higher in the algal suspensions with a rate of $0.015 \text{ mg N L}^{-1} \text{ h}^{-1}$, which may contribute to the eutrophication of the lake. This study provides new molecular insights into the photochemical release of DON from typical internal particles in eutrophic lakes.



Citation: Liu, Y.; Yao, X.

Photochemical Release of Dissolved Organic Nitrogen from Algal Detritus and Sediment Particles in Lake Taihu, China. *Water* **2023**, *15*, 3346. <https://doi.org/10.3390/w15193346>

Academic Editor: Giuseppe Castaldelli

Received: 20 August 2023
Revised: 14 September 2023
Accepted: 19 September 2023
Published: 24 September 2023



Copyright: © 2023 by the authors. Licensee MDPI, Basel, Switzerland. This article is an open access article distributed under the terms and conditions of the Creative Commons Attribution (CC BY) license (<https://creativecommons.org/licenses/by/4.0/>).

Keywords: photodissolution; internal particles; dissolved organic nitrogen (DON); composition; ammonium; Lake Taihu

1. Introduction

Solar-induced conversion of particle organic matter (POM) to the dissolved state, that is, photodissolution, is an important source of dissolved organic carbon (DOC) and dissolved organic nitrogen (DON) in aquatic systems [1,2]. Earlier studies show that POM from multiple sources can release DOC and/or DON when subjected to light exposure. For example, POM in resuspended sediments of rivers, estuaries, and other environments will generate a large amount of dissolved organic matter (DOM) under simulated light exposure [3–5]. Solar irradiation can not only target substances in resuspended sediments similar to terrestrial sources, but can also target biogenic substances such as planktonic algal debris, flocs, etc. Algal debris has a high photoreactivity, with up to 10% of its POM potentially being converted into DOM, and the release of DON dominated the photodissolution of nitrogen, followed by a lower photoammonification process [6]. Both the algal residues and the residues reprocessed by microorganisms in the early stage are prone to photolysis after irradiation [6]. The photodissolution of flocculent or detrital particles from natural water bodies or wastewater treatment plants also resulted in the release of a large amount of DOM [7,8], and the particle size was significantly reduced [7].

Photodissolution of POM potentially increases DOC and total dissolved nitrogen (TDN) loads in estuarine waters by 3–85% and 4–75%, respectively [5]. The easily degradable components of DOM released by POM photodissolution can reach 50% [3]. Thus, POM photodissolution has the potential to provide a substantial pool of dissolved nutrients to affect lake biogeochemical processes [9]. Yet, photoproducts from different POM sources has not been well-characterized, and there are few studies focusing on the production of labile nitrogen (e.g., small DON and dissolved inorganic nitrogen (DIN)), which can limit the lake primary production in eutrophic lakes, especially in warm seasons [10].

Photodissolution of POM most likely affects the biogeochemistry of shallow lakes. Shallow lakes are normally prone to frequent wind wave disturbances, and thus, frequent particulate matter resuspension events, during which internal particles such as algae and sediments have high loads. Studies further show that humic substances play an important role in the photochemical release of DOC, whether imported from upstream (e.g., terrigenous humic) or produced in the benthic environment [11]. Solar-induced release of DON in algal and sediment suspensions may potentially contribute to significant amounts of DON and inorganic nitrogen influencing lake primary production. However, the relative role of algae- and sediment-dominated photodissolution in contributing to DON and DIN releases remains unclear, which limits our understanding of internal nutrient cycling in eutrophic shallow lakes.

We hypothesized that the photochemical release of DON and inorganic nitrogen from algal detritus and sediment particles can potentially be an important internal nutrient source in eutrophic shallow lakes. Thus, main objectives of this study were to: (1) investigate the release rate of dissolved nutrients during the simulated light irradiation of algal detritus and sediment suspensions; (2) provide optical and molecular insights into the changes of DOM and DON compositions. Taken together, the data reveals that algal suspensions can release DON and ammonium (NH_4^+) at substantial rates, which may contribute labile nitrogen available to algal species.

2. Materials and Methods

2.1. Site Description and Sample Collection

Lake Taihu is a large shallow lake with a surface area of 2338 km², which is the third largest freshwater lake in China [12,13]. It is located in one of the most developed areas of China, the Yangtze River Delta, and has a mean depth of 1.9 m [10,12,13]. The lake is an important drinking water source for more than 10 million people in the surrounding big cities such as Wuxi, Suzhou, Shanghai, and Huzhou. The lake also supports a large number of industrial, agricultural, and municipal activities [12,14]. In recent decades the lake became eutrophic as a result of increased human activities and nutrient inputs [12,15]. Meiliang Bay is a semi-enclosed bay located in the northern part of Lake Taihu, where frequent algal blooms occur during warm seasons.

To determine the photodissolution of typical internal POM, we chose to use resuspended sediment and bloom algae (>64 μm) for irradiation experiments as they usually have high loads in the water column. The algae were sampled on 10 August 2022, during a *Cyanobacterial* bloom by towing a phytoplankton net (64 μm) at the platform of Taihu Laboratory for Lake Ecosystem Research (TLLER), Chinese Academy of Sciences, near the coast of Meiliang Bay (Figure 1). Surface sediments (0–2 cm) were sampled from Meiliang Bay in the north of Lake Taihu (120.19433° E, 31.47633° N) on 10 August 2020, using a Peterson's grab sampler (Figure 1). Sediment samples were collected into a ziplock bag and kept frozen at -20°C until experiments commenced.

2.2. Photodissolution Experiments for Algal and Sediment Suspensions

The concentrated algae samples were rinsed with deionized water to remove the attached dissolved matter. To focus on the photodissolution of truly particulate phases, we extracted membrane-rich detritus following Mayer et al. [6]. Briefly, the algae were ultrasonically treated in an ice bath for 2 min, centrifuged to remove the supernatant,

rinsed with deionized water, and centrifuged again. The rinse and centrifugation were repeated several times until the supernatant was clear. The algal membrane-rich detritus was then freeze-dried in a lyophilizer (Biosafer-10A, BioSafer, Nanjing, China), ground gently in a MicroMill, and stored frozen. The time course of photodissolution was tested by irradiating 100 mg L^{-1} suspensions of algal membrane detritus, which were prepared by adding weighed algal detritus to deionized water. Irradiation experiments were conducted in a photo-reactor (Nbet Technology, Beijing, China), which used a 500 W xenon lamp to simulate the solar spectrum. The lamp was put into the center of a quartz hydro pump that used circulated cooling water to keep the temperature stable. The incubation temperature was controlled at $25 \text{ }^{\circ}\text{C} \pm 1 \text{ }^{\circ}\text{C}$. The light intensity near the surface of the quartz tubes was about 21 mW cm^{-2} , close to the daytime light intensity on the surface of the lake water. Prepared algal suspensions were then put into a series of quartz reaction tubes, with each having a sample volume of 70 mL. These tubes were then subjected to simulated light irradiation. Duplicate tubes were taken out from the incubator at 0, 0.5, 1, 2, 4, 6, and 8 h, respectively, for later analyses of nutrient concentrations and DOM/DON compositions.

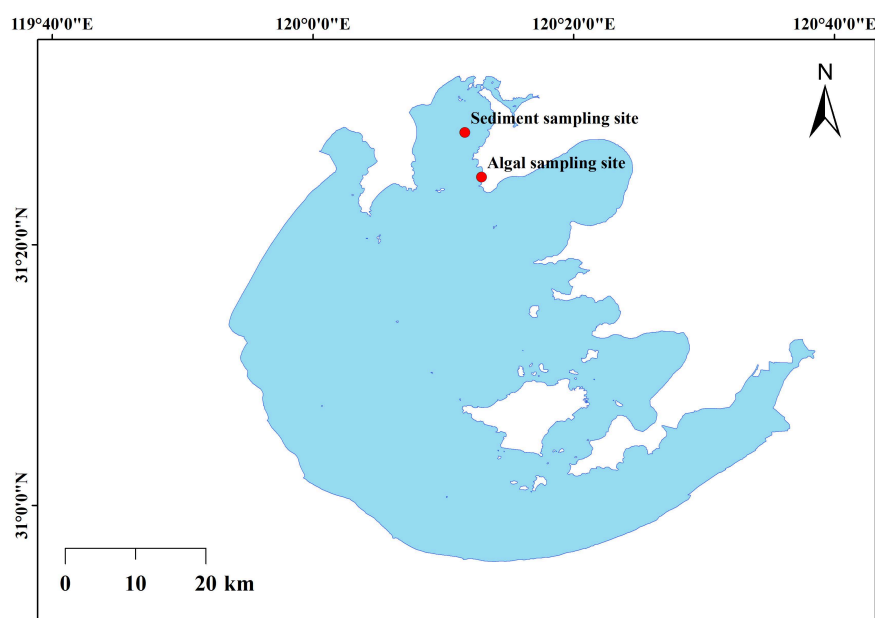


Figure 1. Sampling sites of the algae and sediment used in this study.

Sediments prior to irradiation experiments were freeze-dried, ground, and sieved through a 100 mesh (0.150 mm) sieve. Sediment suspensions were then prepared by mixing 70 mL of deionized water and 35 mg sediments (dry weight, with a concentration of 500 mg L^{-1}) into each quartz tube. The sediment suspensions were then subjected to light irradiation, as described earlier. At 0, 0.5, 1, 2, 4, 6, and 8 h, duplicate quartz tubes were taken out from the incubator for later analysis of nutrient concentrations and DOM/DON compositions.

All samples from the suspensions were filtered through Whatman GF/F (GE Healthcare, Pittsburgh, PA, USA) filters immediately after sampling. The GF/F filters were pre-combusted in a Muffler furnace at $450 \text{ }^{\circ}\text{C}$ for 2 h. Samples for UV-Visible (UV-Vis) absorption spectroscopy and Fourier transform ion cyclotron resonance mass spectrometry (FT-ICR MS) analyses were further filtered through $0.22 \text{ }\mu\text{m}$ porosity membranes (Millipore Sigma, Burlington, VT, USA). Samples at 1-h (sediment incubations) and 8-h (algal detritus and sediment incubations) were not measured for UV-Vis spectroscopy and TDN because they were all used for FI-ICR MS analyses. Samples at 0.5-h and 1-h during algal detritus incubations lost their replicates for UV-Vis spectroscopy measurements due to faulty filtering operations.

2.3. Sample Analyses

2.3.1. Measurements of Nutrient Concentrations

The GF/F filtered samples were measured for dissolved organic carbon (DOC), TDN, NH_4^+ , nitrate (NO_3^-), and nitrite (NO_2^-) concentrations according to the Chinese standard methods for observation of lake eutrophication [16]. Concentrations of TDN were measured using the potassium persulfate digestion procedure, followed by the colorimetric method on a Shimadzu UV-2600 spectrophotometer (Kyoto, Japan) with a detection limit of 0.02 mg L^{-1} . Concentrations of NO_3^- , NO_2^- , and NH_4^+ were measured on a continuous flow analyzer (San⁺⁺, Skalar Analytical B.V., Breda, the Netherlands). The detection limits for NO_3^- , NO_2^- , and NH_4^+ were 0.01 mg L^{-1} , 0.001 mg L^{-1} , and 0.01 mg L^{-1} , respectively. Concentrations of DON were calculated as the difference between TDN and the sum of NO_3^- , NH_4^+ , and NO_2^- , and the standard deviations for DON were calculated using an error propagation method. Concentrations of DOC were analyzed on a Shimadzu total organic carbon analyzer (TOC-V CPN, Kyoto, Japan) using the high-temperature ($\sim 680^\circ\text{C}$) combustion and catalytic oxidation method.

2.3.2. UV-Vis Absorption Spectroscopy

UV-Vis absorption spectroscopy of incubation samples was determined on a Shimadzu UV-2550PC spectrophotometer (Kyoto, Japan) using 5 cm quartz cuvettes. The scan wavelength range was between 200 and 800 nm at 1 nm intervals, and the scan rate was set as 210 nm min^{-1} . Deionized water was run as the blank to test the stability of the instrumental baseline. The absorbance values were transformed into absorbance coefficients according to the following formula [17]:

$$a_{(\lambda)} = 2.303A_{(\lambda)}/r \quad (1)$$

where $A_{(\lambda)}$ is the absorbance at wavelength λ , r is the light path length of the quartz cuvette (0.05 m), and $a_{(\lambda)}$ is the absorbance coefficient (m^{-1}) at wavelength λ . The absorption coefficient at 254 nm ($a(254)$) was used to reflect the abundance of chromophoric dissolved organic matter (CDOM), as described in earlier studies [18,19]. The spectral slopes $S_{275-295}$ and $S_{350-400}$, calculated based on the nonlinear fitting of absorption spectra at 275–295 nm and 350–400 nm [20], respectively, can indicate the source and composition of DOM [21,22]. $S_{275-295}$ normally increases with a decreasing CDOM molecular weight and aromaticity [21–23]. The molecular size of CDOM was evaluated by the ratio of absorption coefficients at 250 to 365 nm [$a(250):a(365)$], and usually, a decreasing ratio can indicate an increasing molecular size or mean molecular weight [21]. The specific ultraviolet absorption at 254 nm (SUVA_{254}), calculated from the ratio of the absorption coefficient at 254 nm to DOC ($a(254)/\text{DOC}$, in $\text{L mg}^{-1} \text{ C m}^{-1}$), can characterize the aromaticity of CDOM, with a larger value of SUVA_{254} indicating a higher aromaticity of the molecules [24,25].

2.3.3. FT-ICR MS Analysis

The filtered samples for FT-ICR MS analysis were adjusted to $\text{pH} = 2$ with HCl (LC-MS grade) to improve the extraction efficiency of organic acids and phenols [26,27]. The acidified DOM was extracted and concentrated using 500 mg, 6 mL solid phase extraction cartridges (Varian Bond Elut PPL, Agilent Technologies, Santa Clara, CA, USA) following the methods described by Dittmar et al. [26]. Operational details can be found in our early study [28]. Briefly, each PPL cartridge was pre-washed with methanol (ULC-MS grade) using twice the volume of the cartridge, and then the acidified samples were loaded onto the PPL cartridge at a flow rate of $\leq 5 \text{ mL min}^{-1}$. After that, two times the volume of the cartridge of 0.01 M HCl was passed through every cartridge to remove salt and residual NH_4^+ , and then the cartridges were blown dry with high-purity N_2 ($\geq 99.999\%$). Finally, DOM on each PPL cartridge was eluted with 1 mL methanol (ULC-MS grade). After solid phase extraction, the methanol extracts were measured using a 9.4 Telsa FT-ICR MS (Bruker, Billerica, MA, USA) at the China University of Petroleum, Beijing, China. To minimize complications due to sodium adduct formation, the samples were analyzed in negative electrospray ionization

mode [29]. The mass measurement precision of assigned formulas was <0.3 ppm after internal calibration. Molecular formulas were assigned to peaks having signal-to-noise ratios >6 [28,30]. Further mass calibration and data processing were conducted following previously reported methods [31,32]. A caution is that the total number of assigned formulas may be underestimated due to the presence of isomers in the samples [33].

The normalized peak intensity of each formula within a sample was calculated as the ratio of individual peak intensity to the total intensity of all formulas. The ultrahigh resolution and mass accuracy (<1 ppm) of FT-ICR MS can identify thousands of molecular formulas from a single DON sample. The assigned molecular formulas were categorized into CHO-, CHON-, and CHOS-composed classes. This study aims to focus on the changes in DON composition, so CHON-composed formulas were used to characterize DON at the molecular level and are mainly described in the main text. The double bond equivalent (DBE) of the formulas was calculated referring to Stubbins et al. [34]. The modified aromaticity index (AI_{mod}) was calculated as described in Koch and Dittmar [35]. Van Krevelen (VK) diagrams were usually used to group the N peaks into several known compound classes [29,36,37]. The VK diagram is a two-dimensional plot with the O/C ratio in the molecular formula as the x -axis and the H/C as the y -axis. The chemical composition of molecules then can be further categorized by the van Krevelen diagram [37], including carbohydrates ($0.67 \leq \text{O/C} \leq 1.2$ and $1.5 \leq \text{H/C} \leq 2.2$), proteins and amino acids ($0.3 \leq \text{O/C} \leq 0.67$ and $1.5 \leq \text{H/C} \leq 2.2$), lipids ($0 \leq \text{O/C} \leq 0.3$ and $1.5 \leq \text{H/C} \leq 2.0$), lignins ($0.1 \leq \text{O/C} \leq 0.67$ and $0.7 \leq \text{H/C} \leq 1.5$), tannins ($0.67 \leq \text{O/C} \leq 1.2$ and $0.5 \leq \text{H/C} \leq 1.5$), unsaturated hydrocarbons ($0 \leq \text{O/C} \leq 0.1$ and $0.7 \leq \text{H/C} \leq 1.5$), condensed aromatics ($0 \leq \text{O/C} \leq 0.67$ and $0.2 \leq \text{H/C} \leq 0.7$), and others.

2.4. Statistical Analyses

Significant differences between parameter means, e.g., at different irradiation times, were evaluated using independent-samples t -test (2-tailed). Relationships between the quantitative or compositional parameters of DOM/DON and the incubation time were evaluated using linear regression analyses or first-order kinetic fittings, which were usually used in earlier studies [38–40]. Variance analyses (ANOVA) were used to test whether the regression slope was significantly different from zero, or whether the fitting function is significantly better than the function $y = \text{constant}$. Relationships and differences were considered to be significant at a p -value of <0.05 . Statistical analyses were finished using Excel in Office 365 (Microsoft, Redmond, WA, USA), SPSS 20.0 (IBM Analytics, Armonk, NY, USA), and OriginPro 2021 (OriginLab Corporation, Northampton, MA, USA), and software packages.

3. Results

3.1. Photochemical Changes in the Properties of Dissolved Organic Matter in the Suspensions

Irradiated algal detritus suspensions showed a rapid release of DOM during an exposure period of 6 h. DOC and DON were released linearly at a rate of $1.17 \text{ mg C L}^{-1} \text{ h}^{-1}$ (Figure 2a, $r = 0.93$, $p < 0.05$) and $0.14 \text{ mg N L}^{-1} \text{ h}^{-1}$ (Figure 2b, $r = 0.88$, $p < 0.05$), respectively. Continuous irradiation resulted in DOC increasing by 209%. The $a(254)$ increased rapidly within 2 h, while remaining relatively stable after 2 h (Figure 2c). The trend of $a(254)$ with incubation time can be fitted using an exponential growth model (Figure 2c, adj. $R^2 = 0.81$, $p < 0.05$). At 2-h, the $a(254)$ increased by 85%. The $S_{275-295}$ displayed an increasing trend with incubation time, but the trend is not significant (Figure 2d). There was a linearly increasing trend in the $a(250):a(365)$ with a rate of 0.17 h^{-1} (Figure 2e), while the SUVA_{254} decreased linearly with a rate of $0.58 \text{ L mg}^{-1} \text{ C m}^{-1}$ (Figure 2f).

During the irradiation of sediment suspensions, the photochemical release rates of DOC and DON were significantly lower than in algal detritus suspensions (Figure 3a,b). The DOC concentrations showed an increasing trend after 0.5-h, while the trend was not significant (Figure 3a, $r = 0.91$, $p > 0.05$). The decrease in DOC at the early stage of the incubation (before 0.5-h) might be because the system had not physically achieved a dissolution equilibrium. Similarly, the DON concentrations also showed no obvious trend

during the incubation (Figure 3b, $p > 0.05$), yet were obviously higher at 6-h than at 4-h. The $a(254)$ showed a significant linear increasing trend (Figure 3c, $r = 0.97$, $p < 0.01$) at a rate of $0.249 \text{ m}^{-1} \text{ h}^{-1}$. The $S_{275-295}$ decreased with the incubation time, and the trend can be better fitted by an exponential model (Figure 3d, adj. $R^2 = 0.97$, $p < 0.05$). The $a(250):a(365)$ showed no significant linear trend with the incubation time (Figure 3e, $p > 0.05$), while the SUVA_{254} increased rapidly within 2 h and remained relatively stable at 2–6 h, which approximately fits an exponential model (Figure 3f, adj. $R^2 = 0.87$, $p = 0.07$).

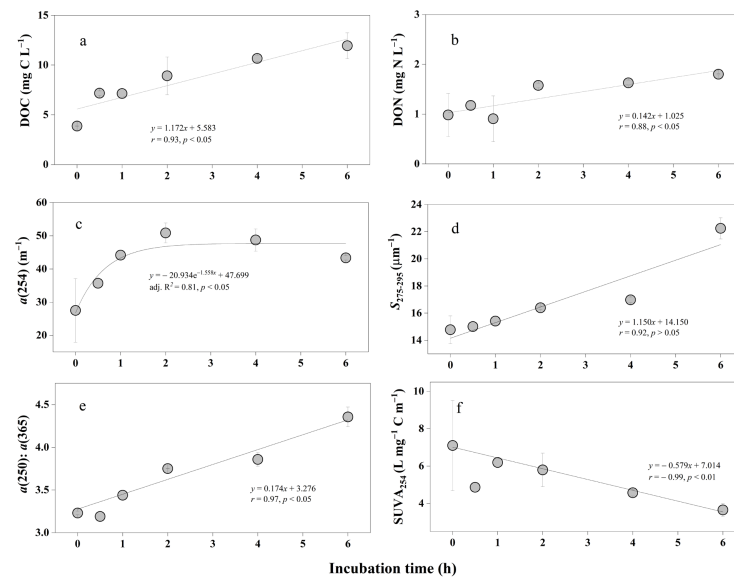


Figure 2. Changes in the dissolved organic carbon (DOC) (a) and dissolved organic nitrogen (DON) (b) concentrations and UV–Visible parameters of DOM in the irradiated algal detritus suspensions. The UV–Visible parameters of DOM include spectral absorption coefficients $a(254)$ (c), spectral slope $S_{275-295}$ (d), molecular size ($a(250):a(365)$) (e), and specific ultraviolet absorption at 254 nm (SUVA_{254}) (f).

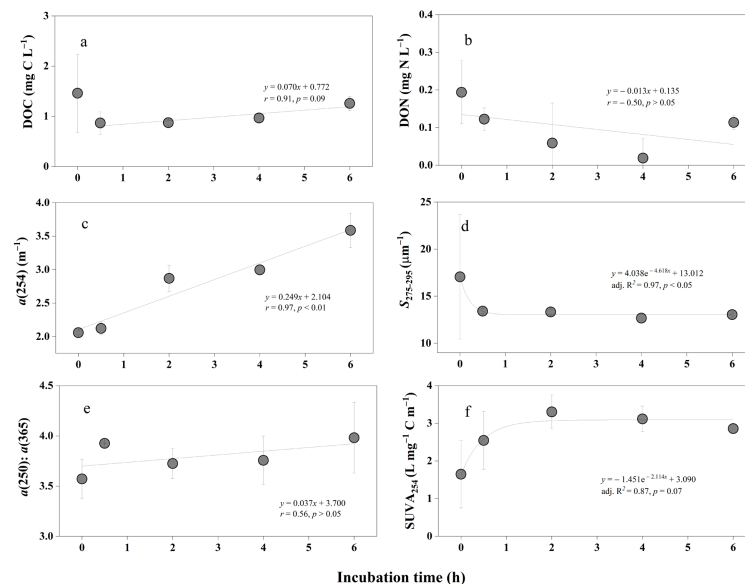


Figure 3. Changes in the dissolved organic carbon (DOC) (a) and dissolved organic nitrogen (DON) (b) concentrations and UV–Visible parameters of DOM in the irradiated sediment suspensions. The UV–Visible parameters of DOM include spectral absorption coefficients $a(254)$ (c), spectral slope $S_{275-295}$ (d), molecular size ($a(250):a(365)$) (e), and specific ultraviolet absorption at 254 nm (SUVA_{254}) (f).

3.2. Photochemical Changes in the Molecular Composition of Dissolved Organic Nitrogen

Compared to the molecular composition of DON at the start of algal incubations, the total number of N-containing formulas increased largely from 1349 to 4135 at 8-h, the average DBE increased from 5.88 to 6.89, and the average N/C increased from 0.09 to 0.10. In addition, average m/z , DBE/C, DBE/H, DBE/O, and AI_{mod} of DON also increased at 8-h, while H/C decreased from 1.54 to 1.47 (Table 1). DON at the start of irradiation was mainly composed of proteins and lignin components, while after an irradiation of 8 h, a large number of new molecules were released, including lipids, proteins and amino acids, tannins, and carbohydrates, etc. (Figure 4a,b and Figure 5a). Lignin showed the largest increase in abundance, followed by carbohydrates and lipids, while the abundance of proteins and amino acids showed the largest decrease (Figure 5c). The number proportions of proteins and amino acids among the total number of formulas decreased from 43% to 35%, while carbohydrates, lipids, and lignin increased from 2% to 6%, 4% to 5%, and 46% to 50%, respectively (Figure 6a). The intensity proportions of each class of N-containing formulas subcategorized by VK plots showed a similar pattern to those of number proportions (Figure 6b). Some larger molecules such as condensed aromatics and unsaturated hydrocarbons were also released after an irradiation of 8 h (Figures 4b and 5a).

Table 1. Changes in the molecular composition of DON (CHON formulas) during the incubation of algae and sediment suspensions upon exposure to simulated sunlight.

Incubations	Total Number of All Formulas	Total Number of CHON Formulas	Average m/z	H/C	O/C	N/C	DBE	AI_{mod}	DBE/C	DBE/H	DBE/O
Algal 0-h	1349	608	397.27	1.54	0.41	0.086	5.88	0.10	0.33	0.25	0.97
Algal 8-h	4135	2625	404.82	1.47	0.42	0.099	6.89	0.14	0.37	0.30	1.09
Sediment 1-h	3426	1431	391.80	1.53	0.38	0.081	6.00	0.13	0.33	0.25	0.96
Sediment 8-h	2222	1092	341.04	1.45	0.38	0.111	6.26	0.21	0.40	0.32	1.19

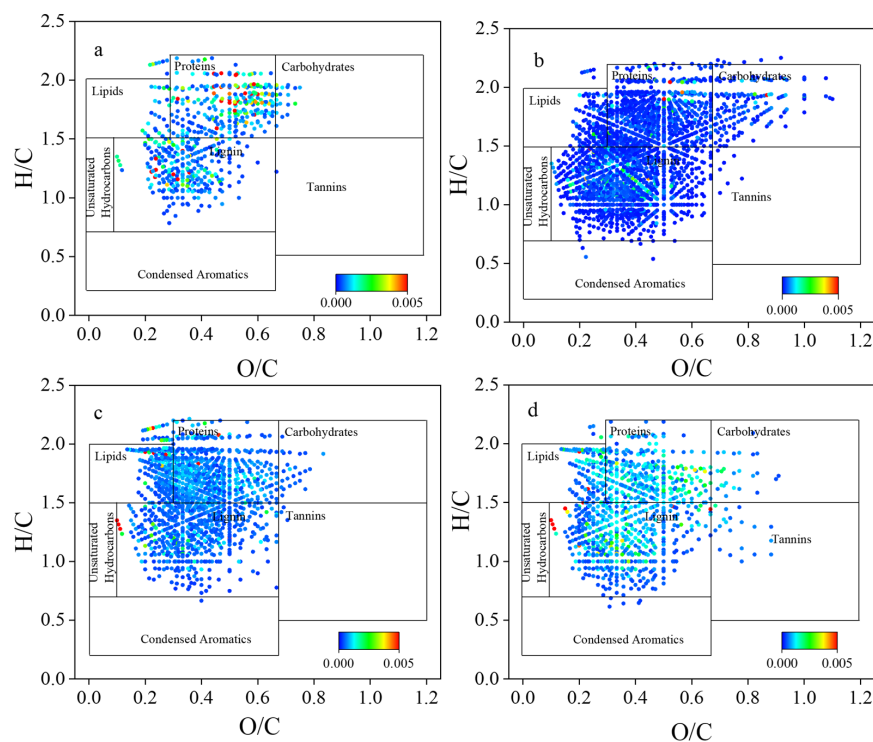


Figure 4. Van Krevelen (VK) plots of N-containing formulae during the incubation of algal (a,b) and sediment (c,d) suspensions upon exposure to simulated sunlight at 0 (a,c), and 8 (b,d) h.

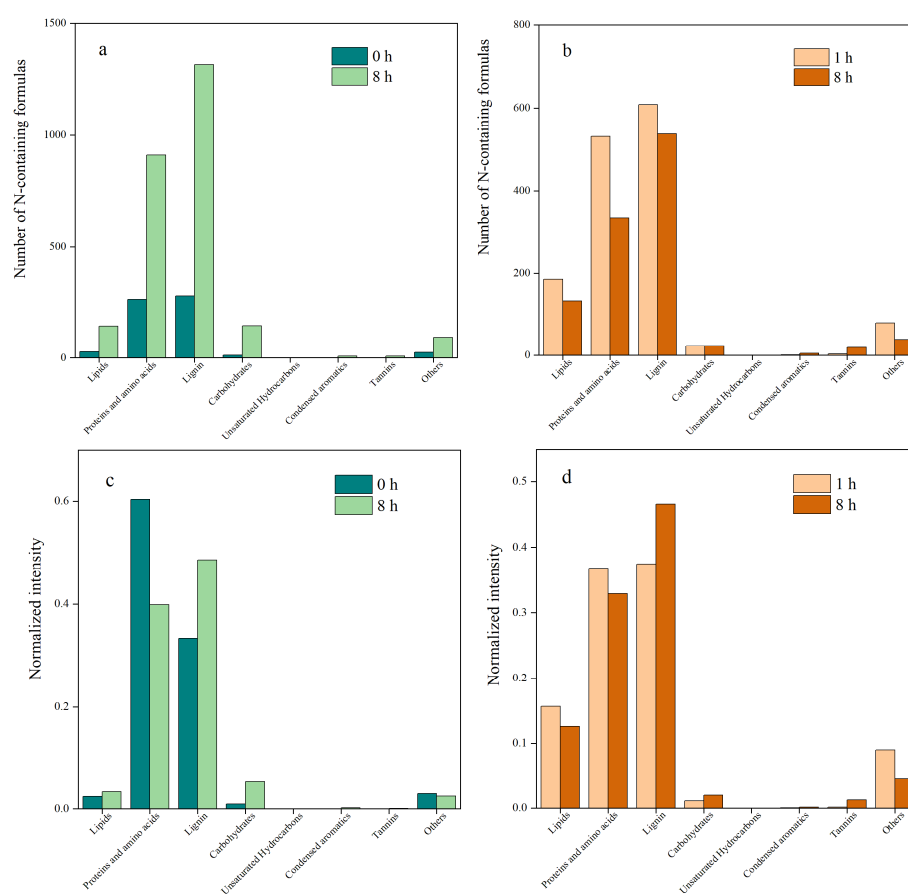


Figure 5. The number (a,b) and normalized intensity (c,d) of N-containing formulas assigned to each compound class in irradiated algal (a,c) and sediment (b,d) suspensions at different incubation time.

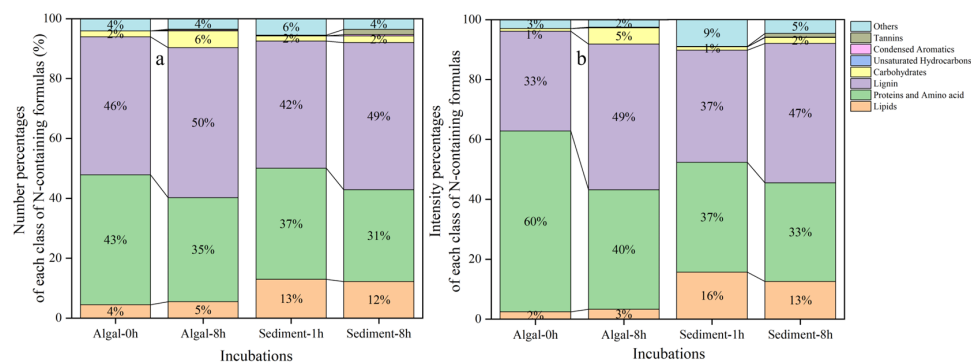


Figure 6. The number (a) and intensity (b) percentages of each class of N-containing formulas subcategorized by van Krevelen (VK) plots in irradiated algal and sediment suspensions at different incubation time.

Changes in the molecular composition of DON during the irradiation of sediment suspensions are also summarized in Figures 4–6 and Table 1. The assigned total number of CHON-formulas decreased from 1431 to 1092 after an irradiation period of 8 h, while the average DBE increased from 6.00 to 6.26, and the average N/C increased from 0.09 to 0.10 (Table 1). In addition, DBE/C, DBE/H, DBE/O, and AI_{mod} of DON also increased at 8-h, while average m/z and H/C decreased (Table 1). DON formulas at the early stage (1 h) of irradiation are mainly composed of lignin (42%), proteins and amino acids (37%), and lipids (13%). After an irradiation of 8 h, the formula number of proteins and amino acids and lipids decreased, yet some lignin, tannin, and condensed aromatic molecules were

produced (Figure 4c,d and 5b). The lignin showed the largest increase in its abundance, followed by tannin (Figure 5d). The number proportions of lipids and proteins and amino acids among the total number of DON formulas decreased from 13% to 12% and 37% to 31%, respectively, while lignin, tannin, and condensed aromatics increased from 42% to 49%, 0.2% to 1.7%, and 0.1% to 0.5%, respectively (Figure 6a). The intensity proportions of each class of N-containing formulas subcategorized by VK plots showed a similar pattern to those of the number proportions (Figure 6b).

3.3. Photochemical Release of Inorganic Nitrogen during the Irradiation of Algal and Sediment Suspensions

During the irradiation of algal suspensions, NH_4^+ concentrations showed a significant linear increasing trend (Figure 7a, $r = 0.95$, $p < 0.05$) with a rate of $0.015 \text{ mg L}^{-1} \text{ h}^{-1}$, while NO_3^- concentrations decreased linearly at a quite low rate of $0.007 \text{ mg L}^{-1} \text{ h}^{-1}$ (Figure 7b, $r = -0.93$, $p < 0.01$). NH_4^+ concentrations increased by 161% within an irradiation period of 8 h. The release of NO_2^- showed no significant linear trend with irradiation time (Figure 7c, $p > 0.05$). During the irradiation of sediment suspensions, NH_4^+ concentrations also showed an increasing trend (Figure 7d, $r = 0.71$, $p = 0.07$) with a photoammonification rate of $0.002 \text{ mg L}^{-1} \text{ h}^{-1}$. The release of NO_3^- showed no significant linear trend with irradiation time (Figure 7e, $p > 0.05$), while NO_2^- concentrations increased linearly during the incubation (Figure 7f, $r = 0.83$, $p < 0.05$) with a quite low rate of $0.0006 \text{ mg L}^{-1} \text{ h}^{-1}$. The photoammonification rates in the algal suspensions were much higher than in the sediment suspensions.

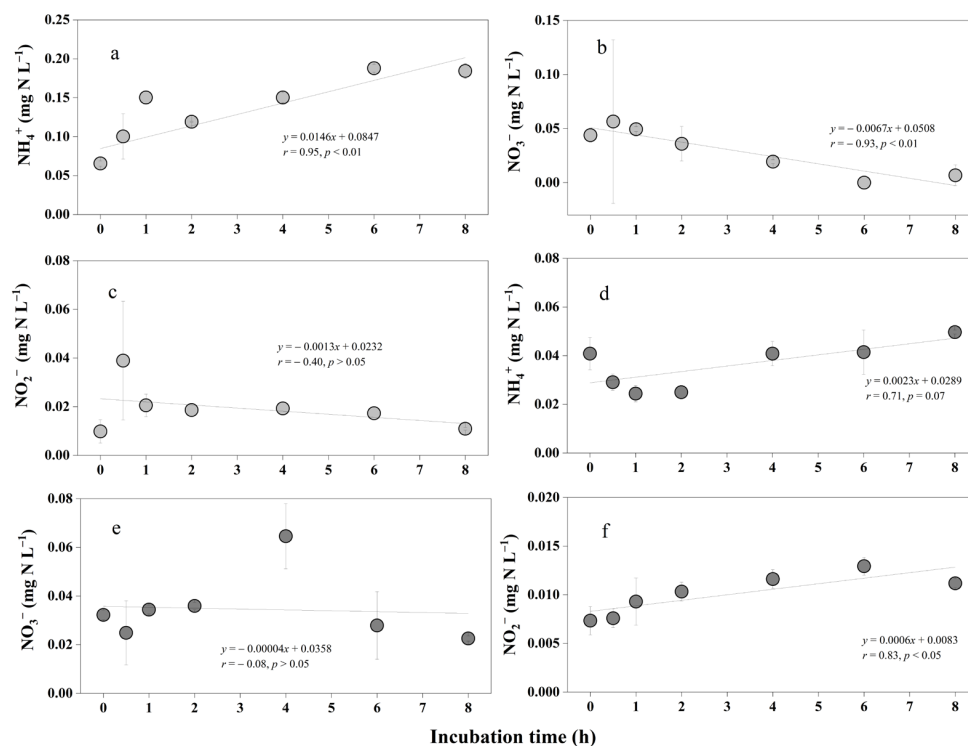


Figure 7. Photochemical release of inorganic nutrients from algal detritus (a–c) and sediment (d–f) particle suspensions.

4. Discussion

4.1. Photochemical Release of Dissolved Organic Nitrogen from Algal and Sediment Particles

After simulated solar irradiation for 6 h, up to ten percent of POM from algal detritus converted to photo-dissolved organic matter (DOC achieved to 12 mg L^{-1}), in which DON dominated the nitrogen photodissolution, followed by photoammonification (Figures 2, 4 and 7). Algal intracellular and extracellular organic matter is rich in highly

labile protein-like components [41,42]. This study further shows that proteins and amino acids, having decreased percentages among total formulas, may play an important role in the release of many other molecules, e.g., lignin and carbohydrates (Table 1). The mechanism of photodissolution may be similar to the photochemical reaction after DOM absorbs light, involving direct photolysis reactions between light and POM components and secondary photochemical processes, including reactive intermediate production, e.g., reactive oxygen species (ROS). Pigments, proteins (such as aromatic structural proteins and tryptophan-like proteins), and unsaturated lipids are likely sources of reactive oxygen species (ROS) via photosensitization reactions, which indirectly induce POM dissolution [6,43]. Thus, although photohumification reactions produced some larger humic-like and aromatic DON molecules (Figure 4a,b and Figure 5a,c and Table 1), the whole DOM pool showed decreasing aromaticity and molecular size with the irradiation time (Figure 2). These results suggest that photodissolution of algal detritus potentially releases large amounts of small labile DON components that will accelerate the eutrophication of the lake.

In the irradiated sediment suspensions, the release rate of DOC ($\sim 1.68 \text{ mg L}^{-1} \text{ d}^{-1}$, after 0.5-h) is more intense than that of DIN species (Figures 3 and 7), which is consistent with the findings in river ecosystems [1]. POM in resuspended sediments of rivers, estuaries, and other environments will generate a large amount of DOM under simulated natural light exposure [3–5], which can make the DOC and TDN loads of estuary waters increase by 3–85% and 4–75%, respectively [5]. The photodissolution of POM from resuspended sediments is a significant source of DON while not contributing significantly to DIN [1]. The DON concentrations in this study did not show a significant increasing trend with irradiation time (Figure 3b), probably because of a short incubation time (e.g., an increasing trend of DON was shown from 4-h to 6-h) and/or a combination of analyses errors of several nitrogen species in DON. However, the results clearly suggested that the diversity of molecular formulas decreased, with more aromatic, condensed, and humic-like molecules produced (e.g., lignin, condensed aromatics, and tannins, Figures 3 and 4 and Table 1). The humic component of resuspended sediments may play an important role in releasing organic matter via photodissolution [11], which also involves in direct photolysis reactions and secondary photochemical processes as mentioned earlier. Photodegradation of sediment-derived organic matter reduces its ability to generate ROS further due to reduced light absorption [19]. Thus, most photodissolved DON molecules from the sediment suspension might be less bioavailable to microbes than those from algal suspensions.

4.2. Photochemical Release of Inorganic Nitrogen from Algal and Sediment Particles

Photochemical release of NH_4^+ was faster in the irradiated algal suspensions ($0.312 \text{ mg L}^{-1} \text{ d}^{-1}$ at an algal debris concentration of 100 mg L^{-1}) than in sediment suspensions, indicating that photoammonification rates may relate to the composition of POM. As mentioned earlier, algal debris contains more protein-like components and amino groups, which, upon irradiation, can have higher hydroxyl radical (OH) quantum yields than terrigenous or sediment sources [43,44]. The reactive oxygen species OH \cdot not only promotes the degradation of organic matter but can also intensify the photoammonification process of amino acids [44]. During photoammonification, amide bonds in the peptide first undergo photochemical cleavage to generate primary amines, which are then hydrolyzed to NH_4^+ [45]. Therefore, planktonic algal detritus has many photosensitive substances in its components, which may be directly or indirectly photochemically degraded and transformed. The degraded DON components were mainly lipids and proteins and amino acids, and the aromatic and heterocyclic amino acids produced more NH_4^+ than other amino acids [44]. The photoammonification process plays a key role in the conversion of DON to DIN, and its products were found to have a significant impact on bacterial biomass [46]. In the sediment suspensions, however, continuous light exposure led to insignificant changes in the concentrations of NH_4^+ and NO_3^- , possibly indicating that the photodissolution of sediment particles to produce inorganic nitrogen is relatively slow.

4.3. Implications for Eutrophication Control

This study shows that sunlight can cause significant dissolution of organic matter from sediments to relatively young organic matter, algal detritus. In the past two decades, harmful algal blooms frequently occurred in Lake Taihu due to accelerated eutrophication and climate change, and up to 25% of the lake area can be covered by “floating algae” [15,47]. The blooms initiated in spring and persisted well into fall [48], and during the blooms, dissolved inorganic nitrogen is quite limited [49]. Yet, a growing body of evidence shows that algae species can utilize DON similar to inorganic N [50–52]. Furthermore, cyanobacteria are more competitive than some other algae species in utilizing DON [53], especially when inorganic N concentrations are low. In Lake Taihu, DON may play an increasingly important role in the persistence of cyanobacterial blooms [10]. Therefore, even if the concentration of inorganic nitrogen was controlled at a lower level, high DON concentrations may still support the bloom persistence as important nitrogen nutrition. Thus, photodissolved DON and NH_4^+ from algal detritus may contribute to significant bioavailable N in surface waters during warm seasons of high radiation and low inorganic nitrogen concentrations, with the potential to influence nutrient dynamics in the lake. Furthermore, large shallow lakes such as Lake Taihu are vulnerable to wind-related wave disturbances, and surface sediment resuspensions occur frequently. The photodissolution of resuspended sediments in the surface layer of the lake may thus become an important source of DOC and/or DON, most of which are available for microbial uptake [6]. Our results provide molecular insights into the photodissolution of sediment particles and relatively young algal organic matter detritus.

It is still uncertain whether the photodissolution of internal particles has the potential to affect lake primary production. The irradiation experiments for algal detritus or sediment suspensions in this study were conducted at high concentrations of 100 and 500 mg L^{-1} in deionized water, respectively. Many conditions may affect the applicability of results in the current study to field conditions, e.g., light environment, lake hydrodynamics, lake photosensitive substances, algal growth stages, etc. In addition, we did not test the influence of any of the sample processing steps on the results, while an earlier study shows that up to 2 years freezing storage of the algal detritus has a small impact on the results [6]. Although sample processing steps such as ultrasonic processing and freeze-drying may have the potential to disrupt algal cell walls and influence the release of DON, our experiments facilitate the revelation of internal nutrient sources of dissolved nutrients, which are important nutrient regeneration mechanisms and contribute to algal bloom persistence in Taihu Lake. Future studies should address the photoreactivity of POM from different algal substrates and examine its interactions with the photolysis of other particles, e.g., humic-rich terrigenous and sediment sources, combining ROS analysis.

5. Conclusions

This study investigates the photochemical release and alteration of DON during the simulated solar irradiation of two typical types of internal particles in Lake Taihu, China. Results showed that both irradiated algal detritus and sediment suspensions have a continuous release of DOM. Algal suspensions had high photoreactivity and released a larger number of new DON molecules with low molecular weight and aromaticity (e.g., carbohydrates and lipids), potentially available to plankton in the lake. In addition, higher photoammonification rates were found in algal suspensions. The protein and amino acid composition may play an important role in the photodissolution mechanism of POM from algal detritus. Irradiated sediment suspensions, however, showed decreased diversity of DON formulas, and the DON tended to be more aromatic, condensed, and humic-like. A short irradiation period of 8 h for sediment suspensions did not result in significant photoammonification rates. Therefore, photodissolution of algal detritus may contribute to more diverse and labile DON, especially during harmful algal blooms. Yet, the bioavailability of photodissolved DON from algal detritus and resuspended sediments needs to be studied further in the future.

Author Contributions: Conceptualization, X.Y.; methodology, Y.L. and X.Y.; software, Y.L. and X.Y.; validation, Y.L. and X.Y.; formal analysis, Y.L. and X.Y.; investigation, Y.L.; resources, X.Y.; data curation, Y.L. and X.Y.; writing—original draft preparation, Y.L. and X.Y.; writing—review and editing, Y.L. and X.Y.; visualization, Y.L. and X.Y.; supervision, X.Y.; project administration, X.Y.; funding acquisition, X.Y. All authors have read and agreed to the published version of the manuscript.

Funding: This research was funded by the Natural Science Foundation of Jiangsu Province in China (grant number BK20201098).

Data Availability Statement: The data used in this study are available upon request.

Acknowledgments: We thank Taihu Laboratory for Lake Ecosystem Research (TLLER), Chinese Academy of Sciences, for providing the platform of algal sampling. The authors are also grateful to the two anonymous reviewers for their constructive comments and suggestions.

Conflicts of Interest: The authors declare no conflict of interest.

References

- Riggsbee, J.A.; Orr, C.H.; Leech, D.M.; Doyle, M.W.; Wetzel, R.G. Suspended sediments in river ecosystems: Photochemical sources of dissolved organic carbon, dissolved organic nitrogen, and adsorptive removal of dissolved iron. *J. Geophys. Res. Biogeosci.* **2008**, *113*, G03019. [[CrossRef](#)]
- Maie, N.; Pisani, O.; Jaff , R. Mangrove tannins in aquatic ecosystems: Their fate and possible influence on dissolved organic carbon and nitrogen cycling. *Limnol. Oceanogr.* **2008**, *53*, 160–171. [[CrossRef](#)]
- Mayer, L.M.; Thornton, K.H.; Schick, L.L. Bioavailability of organic matter photodissolved from coastal sediments. *Aquat. Microb. Ecol.* **2011**, *64*, 275–284. [[CrossRef](#)]
- Mayer, L.M.; Schick, L.L.; Skorko, K.; Boss, E. Photodissolution of particulate organic matter from sediments. *Limnol. Oceanogr.* **2006**, *51*, 1064–1071. [[CrossRef](#)]
- Liu, Q.; Shank, G.C. Solar radiation-enhanced dissolution (photodissolution) of particulate organic matter in Texas estuaries. *Estuaries Coasts* **2015**, *38*, 2172–2184. [[CrossRef](#)]
- Mayer, L.M.; Schick, L.L.; Hardy, K.R.; Estapa, M.L. Photodissolution and other photochemical changes upon irradiation of algal detritus. *Limnol. Oceanogr.* **2009**, *54*, 1688. [[CrossRef](#)]
- Yang, X.; Li, Z.; Meng, F.; Wang, Z.; Sun, L. Photochemical alteration of biogenic particles in wastewater effluents. *Chin. Sci. Bull.* **2014**, *59*, 3659–3668. [[CrossRef](#)]
- Pisani, O.; Yamashita, Y.; Jaff , R. Photo-dissolution of flocculent, detrital material in aquatic environments: Contributions to the dissolved organic matter pool. *Water Res.* **2011**, *45*, 3836–3844. [[CrossRef](#)]
- Shank, G.; Evans, A.; Yamashita, Y.; Jaff , R. Solar radiation-enhanced dissolution of particulate organic matter from coastal marine sediments. *Limnol. Oceanogr.* **2011**, *56*, 577–588. [[CrossRef](#)]
- Yao, X.; Zhang, Y.; Zhang, L.; Zhu, G.; Qin, B.; Zhou, Y.; Xue, J. Emerging role of dissolved organic nitrogen in supporting algal bloom persistence in Lake Taihu, China: Emphasis on internal transformations. *Sci. Total Environ.* **2020**, *736*, 139497. [[CrossRef](#)]
- Hu, B.; Wang, P.; Zhang, N.; Wang, C.; Ao, Y. Photoproduction of dissolved organic carbon and inorganic nutrients from resuspended lake sediments. *Environ. Sci. Pollut. Res.* **2016**, *23*, 22126–22135. [[CrossRef](#)] [[PubMed](#)]
- Qin, B.; Xu, P.; Wu, Q.; Luo, L.; Zhang, Y. Environmental issues of lake Taihu, China. *Hydrobiologia* **2007**, *581*, 3–14. [[CrossRef](#)]
- Chen, Y.; Fan, C.; Teubner, K.; Dokulil, M. Changes of nutrients and phytoplankton chlorophyll-a in a large shallow lake, Taihu, China: An 8-year investigation. *Hydrobiologia* **2003**, *506–509*, 273–279. [[CrossRef](#)]
- Guo, L. Doing battle with the green monster of Taihu Lake. *Science* **2007**, *317*, 1166. [[CrossRef](#)] [[PubMed](#)]
- Chen, Y.; Qin, B.; Teubner, K.; Dokulil, M.T. Long-term dynamics of phytoplankton assemblages: Microcystis-domination in Lake Taihu, a large shallow lake in China. *J. Plankton Res.* **2003**, *25*, 445–453. [[CrossRef](#)]
- Jin, X.; Tu, Q. *The Standard Methods for Observation and Analysis in Lake Eutrophication*; Chinese Environmental Science Press: Beijing, China, 1990. (In Chinese)
- Green, S.A.; Blough, N.V. Optical absorption and fluorescence properties of chromophoric dissolved organic matter in natural waters. *Limnol. Oceanogr.* **1994**, *39*, 1903–1916. [[CrossRef](#)]
- Stedmon, C.A.; Granskog, M.; Dodd, P.A. An approach to estimate the freshwater contribution from glacial melt and precipitation in East Greenland shelf waters using colored dissolved organic matter (CDOM). *J. Geophys. Res. Ocean.* **2015**, *120*, 1107–1117. [[CrossRef](#)]
- Zhang, Y.; Zhou, L.; Zhou, Y.; Zhang, L.; Yao, X.; Shi, K.; Jeppesen, E.; Yu, Q.; Zhu, W. Chromophoric dissolved organic matter in inland waters: Present knowledge and future challenges. *Sci. Total Environ.* **2021**, *759*, 143550. [[CrossRef](#)]
- Stedmon, C.A.; Markager, S.; Kaas, H. Optical properties and signatures of chromophoric dissolved organic matter (CDOM) in Danish coastal waters. *Estuar. Coast. Shelf Sci.* **2000**, *51*, 267–278. [[CrossRef](#)]
- Helms, J.R.; Stubbins, A.; Ritchie, J.D.; Minor, E.C.; Kieber, D.J.; Mopper, K. Absorption spectral slopes and slope ratios as indicators of molecular weight, source, and photobleaching of chromophoric dissolved organic matter. *Limnol. Oceanogr.* **2008**, *53*, 955–969. [[CrossRef](#)]

22. Fichot, C.G.; Benner, R. A novel method to estimate DOC concentrations from CDOM absorption coefficients in coastal waters. *Geophys. Res. Lett.* **2011**, *38*, L03610. [[CrossRef](#)]
23. Fichot, C.G.; Benner, R. The spectral slope coefficient of chromophoric dissolved organic matter (S275–295) as a tracer of terrigenous dissolved organic carbon in river-influenced ocean margins. *Limnol. Oceanogr.* **2012**, *57*, 1453–1466. [[CrossRef](#)]
24. Kothawala, D.N.; von Wachenfeldt, E.; Koehler, B.; Tranvik, L.J. Selective loss and preservation of lake water dissolved organic matter fluorescence during long-term dark incubations. *Sci. Total Environ.* **2012**, *433*, 238–246. [[CrossRef](#)] [[PubMed](#)]
25. Weishaar, J.L.; Aiken, G.R.; Bergamaschi, B.A.; Fram, M.S.; Fujii, R.; Mopper, K. Evaluation of specific ultraviolet absorbance as an indicator of the chemical composition of reactivity of dissolved organic matter. *Environ. Sci. Technol.* **2003**, *37*, 4702–4708. [[CrossRef](#)] [[PubMed](#)]
26. Dittmar, T.; Koch, B.; Hertkorn, N.; Kattner, G. A simple and efficient method for the solid-phase extraction of dissolved organic matter (SPE-DOM) from seawater. *Limnol. Oceanogr. Methods* **2008**, *6*, 230–235. [[CrossRef](#)]
27. Osborne, D.M.; Podgorski, D.C.; Bronk, D.A.; Roberts, Q.; Sipler, R.E.; Austin, D.; Bays, J.S.; Cooper, W.T. Molecular-level characterization of reactive and refractory dissolved natural organic nitrogen compounds by atmospheric pressure photoionization coupled to Fourier transform ion cyclotron resonance mass spectrometry. *Rapid Commun. Mass Spectrom.* **2013**, *27*, 851–858. [[CrossRef](#)]
28. Zhou, Y.; Li, Y.; Yao, X.; Ding, W.; Zhang, Y.; Jeppesen, E.; Zhang, Y.; Podgorski, D.C.; Chen, C.; Ding, Y.; et al. Response of chromophoric dissolved organic matter dynamics to tidal oscillations and anthropogenic disturbances in a large subtropical estuary. *Sci. Total Environ.* **2019**, *662*, 769–778. [[CrossRef](#)]
29. Mesfioui, R.; Abdulla, H.A.N.; Hatcher, P.G. Photochemical alterations of natural and anthropogenic dissolved organic nitrogen in the York River. *Environ. Sci. Technol.* **2015**, *49*, 159–167. [[CrossRef](#)]
30. Zhou, Y.; Xiao, Q.; Yao, X.; Zhang, Y.; Zhang, M.; Shi, K.; Lee, X.; Podgorski, D.C.; Qin, B.; Spencer, R.G.M.; et al. Accumulation of terrestrial dissolved organic matter potentially enhances dissolved methane levels in eutrophic Lake Taihu, China. *Environ. Sci. Technol.* **2018**, *52*, 10297–10306. [[CrossRef](#)]
31. He, C.; Pan, Q.; Li, P.; Xie, W.; He, D.; Zhang, C.; Shi, Q. Molecular composition and spatial distribution of dissolved organic matter (DOM) in the Pearl River Estuary, China. *Environ. Chem.* **2020**, *17*, 240–251. [[CrossRef](#)]
32. Shi, Q.; Pan, N.; Long, H.; Cui, D.; Guo, X.; Long, Y.; Chung, K.H.; Zhao, S.; Xu, C.; Hsu, C.S. Characterization of Middle-Temperature Gasification Coal Tar. Part 3: Molecular Composition of Acidic Compounds. *Energy Fuels* **2013**, *27*, 108–117. [[CrossRef](#)]
33. Feng, S.; Zhang, L.; Wang, S.R.; Nadykto, A.B.; Xu, Y.S.; Shi, Q.; Jiang, B.; Qian, W.B. Characterization of dissolved organic nitrogen in wet deposition from Lake Erhai basin by using ultrahigh resolution FT-ICR mass spectrometry. *Chemosphere* **2016**, *156*, 438–445. [[CrossRef](#)]
34. Stubbins, A.; Spencer, R.G.M.; Chen, H.; Hatcher, P.G.; Mopper, K.; Hernes, P.J.; Mwamba, V.L.; Mangangu, A.M.; Wabakanghanzi, J.N.; Six, J. Illuminated darkness: Molecular signatures of Congo River dissolved organic matter and its photochemical alteration as revealed by ultrahigh precision mass spectrometry. *Limnol. Oceanogr.* **2010**, *55*, 1467–1477. [[CrossRef](#)]
35. Koch, B.P.; Dittmar, T. From mass to structure: An aromaticity index for high-resolution mass data of natural organic matter. *Rapid Commun. Mass Spectrom.* **2006**, *20*, 926–932. [[CrossRef](#)]
36. Kim, S.; Kramer, R.W.; Hatcher, P.G. Graphical Method for Analysis of Ultrahigh-Resolution Broadband Mass Spectra of Natural Organic Matter, the Van Krevelen Diagram. *Anal. Chem.* **2003**, *75*, 5336–5344. [[CrossRef](#)]
37. Ohno, T.; Parr, T.B.; Gruselle, M.C.c.I.; Fernandez, I.J.; Sleighter, R.L.; Hatcher, P.G. Molecular composition and biodegradability of soil organic matter: A case study comparing two New England forest types. *Environ. Sci. Technol.* **2014**, *48*, 7229–7236. [[CrossRef](#)]
38. Porcal, P.; Dillon, P.J.; Molot, L.A. Photochemical production and decomposition of particulate organic carbon in a freshwater stream. *Aquat. Sci.* **2013**, *75*, 469–482. [[CrossRef](#)]
39. von Wachenfeldt, E.; Sobek, S.; Bastviken, D.; Tranvik, L.J. Linking allochthonous dissolved organic matter and boreal lake sediment carbon sequestration: The role of light-mediated flocculation. *Limnol. Oceanogr.* **2008**, *53*, 2416–2426. [[CrossRef](#)]
40. Porcal, P.; Kopáček, J.; Tomková, I. Seasonal Photochemical Transformations of Nitrogen Species in a Forest Stream and Lake. *PLoS ONE* **2015**, *9*, e116364. [[CrossRef](#)] [[PubMed](#)]
41. Li, L.; Gao, N.; Deng, Y.; Yao, J.; Zhang, K. Characterization of intracellular & extracellular algae organic matters (AOM) of *Microcystis aeruginosa* and formation of AOM-associated disinfection byproducts and odor & taste compounds. *Water Res.* **2012**, *46*, 1233–1240. [[PubMed](#)]
42. Nguyen, M.L.; Westerhoff, P.; Baker, L.A.; Hu, Q.; Esparzasoto, M.; Sommerfeld, M.R. Characteristics and Reactivity of Algae-Produced Dissolved Organic Carbon. *J. Environ. Eng.* **2005**, *131*, 1574–1582. [[CrossRef](#)]
43. Niu, X.-Z.; Croué, J.-P. Photochemical production of hydroxyl radical from algal organic matter. *Water Res.* **2019**, *161*, 11–16. [[CrossRef](#)]
44. Zhang, Y.; Zhang, R.; Li, S.-L.; Mostofa, K.M.G.; Fu, X.; Ji, H.; Liu, W.; Sun, P. Photo-ammonification of low molecular weight dissolved organic nitrogen by direct and indirect photolysis. *Sci. Total Environ.* **2021**, *764*, 142930. [[CrossRef](#)] [[PubMed](#)]
45. Wang, W.; Tarr, M.A.; Bianchi, T.S.; Engelhaupt, E. Ammonium photoproduction from aquatic humic and colloidal matter. *Aquat. Geochem.* **2000**, *6*, 275–292. [[CrossRef](#)]

46. Pisani, O.; Boyer, J.N.; Podgorski, D.C.; Thomas, C.R.; Coley, T.; Jaffé, R. Molecular composition and bioavailability of dissolved organic nitrogen in a lake flow-influenced river in south Florida, USA. *Aquat. Sci.* **2017**, *79*, 891–908. [[CrossRef](#)]
47. Deng, J.; Qin, B.; Paerl, H.W.; Zhang, Y.; Ma, J.; Chen, Y. Earlier and warmer springs increase cyanobacterial (*Microcystis* spp.) blooms in subtropical Lake Taihu, China. *Freshw. Biol.* **2014**, *59*, 1076–1085. [[CrossRef](#)]
48. Liu, X.; Lu, X.; Chen, Y. The effects of temperature and nutrient ratios on *Microcystis* blooms in Lake Taihu, China: An 11-year investigation. *Harmful Algae* **2011**, *10*, 337–343. [[CrossRef](#)]
49. Xu, H.; Paerl, H.W.; Qin, B.; Zhu, G.; Gao, G. Nitrogen and phosphorus inputs control phytoplankton growth in eutrophic Lake Taihu, China. *Limnol. Oceanogr.* **2010**, *55*, 420–432. [[CrossRef](#)]
50. Bronk, D.A.; See, J.H.; Bradley, P.; Killberg, L. DON as a source of bioavailable nitrogen for phytoplankton. *Biogeosciences* **2007**, *4*, 283–296. [[CrossRef](#)]
51. Lomas, M.W.; Mark Trice, T.; Glibert, P.M.; Bronk, D.A.; McCarthy, J.J. Temporal and spatial dynamics of urea uptake and regeneration rates and concentrations in Chesapeake Bay. *Estuaries* **2002**, *25*, 469–482. [[CrossRef](#)]
52. Feng, W.; Liu, S.; Li, C.; Li, X.; Song, F.; Wang, B.; Chen, H.; Wu, F. Algal uptake of hydrophilic and hydrophobic dissolved organic nitrogen in the eutrophic lakes. *Chemosphere* **2019**, *214*, 295–302. [[CrossRef](#)] [[PubMed](#)]
53. Glibert, P.M.; Heil, C.A.; Hollander, D.; Revilla, M.; Hoare, A.; Alexander, J.; Murasko, S. Evidence for dissolved organic nitrogen and phosphorus uptake during a cyanobacterial bloom in Florida Bay. *Mar. Ecol. Prog. Ser.* **2004**, *280*, 73–83. [[CrossRef](#)]

Disclaimer/Publisher’s Note: The statements, opinions and data contained in all publications are solely those of the individual author(s) and contributor(s) and not of MDPI and/or the editor(s). MDPI and/or the editor(s) disclaim responsibility for any injury to people or property resulting from any ideas, methods, instructions or products referred to in the content.